Acta Crystallographica Section D
Biological Crystallography
ISSN 0907-4449

Spherical plant viruses: interactions in solution, phase diagrams and crystallization of brome mosaic virus

Marina Casselyn,[a] Javier Perez,[b] Annette Tardieu,[c] Patrice Vachette,[b] Jean Witz[d] and Hervé Delacroix[a]*

[a]Bio Informatique Structurale, Centre de Génétique Moléculaire, Laboratoire Associé à l'Université Pierre et Marie Curie, Case 11, Université Pierre et Marie Curie, 7 Quai St Bernard, 75252 Paris CEDEX 05, France, [b]Laboratoire pour l'Utilisation du Rayonnement Electromagnétique (LURE), Centre Universitaire Paris-Sud, Bâtiment 209D, BP 34, 91898 Orsay CEDEX, France, [c]Laboratoire de Minéralogie et Cristallographie de Paris (LMCP), Case 115, CNRS-UPMC, 4 Place Jussieu, 75252 Paris CEDEX 05, France, and [d]Institut de Biologie Moléculaire et Cellulaire (IBMC), 15 Rue René Descartes, 67084 Strasbourg CEDEX, France

Correspondence e-mail: herve.delacroix@snv.jussieu.fr

Received 10 May 2001
Accepted 12 September 2001

Brome mosaic virus (BMV) is a small icosahedral plant virus of mean diameter 268 Å. Interactions between BMV particles in solution were studied by means of small-angle X-ray scattering in order to find crystallization conditions. The interactions between biomacromolecules as large as these viruses have not yet been systematically studied by this method. As it is known that usually proteins crystallize in, or close to, attractive regimes, the interactions between BMV particles in solution were studied as a function of pH, type of salt and size and concentration of polyethylene glycol. An unexpected result of these studies is that the precipitates obtained upon addition of PEG alone or PEG combined with salt were in fact made of microcrystals, which were all characterized by the same series of diffraction peaks, with positions close to those of a centered cubic space group. A phase diagram of the virus as a function of PEG concentration was established by means of microbatch experiments. From the precipitation zones, conditions for crystallization were tested from 5 to 40 mg ml^{-1} virus with 3–10%(*w*/*v*) PEG 8000 or PEG 20 000. Small crystals were obtained in several conditions after a few days and continued growing for several weeks.

1. Introduction

Brome mosaic virus (BMV) is a small spherical plant virus (Fig. 1) of the bromovirus group of the Bromoviridae family. The BMV capsid, with a mean diameter of 268 Å, is made of 180 copies of a unique protein (20 384 Da, 189 amino acids; SwissProt accession No. P03602) assembled in an icosahedral structure with triangulation number $T = 3$. In common with the other members of its family, BMV possesses a single-stranded RNA genome, divided into four RNAs of molecular weights 1.09, 0.999, 0.7 and 0.3 MDa, respectively. Particles contain either one copy of one of the larger RNAs or one copy of each of the two shorter RNAs, encapsulated in three identical capsids which are all requisite for infection. The three types of particles possess very similar properties and cannot be separated from each other by any physical or chemical technique. At pH values higher than 7, BMV particles swell. This swelling is associated with the release of Ca^{2+} ions and corresponds to an early step of the uncoating process (Brisco *et al.*, 1986; Incardona & Kaesberg, 1964). The BMV structure has already been determined at low resolution by small-angle neutron scattering (Chauvin *et al.*, 1978; Jacrot *et al.*, 1977; Zulauf *et al.*, 1983) and by cryo-electron microscopy and image reconstruction (Krol *et al.*, 1999). The most detailed model of BMV, that of Zulauf *et al.* (1983), is a hollow five-shelled isometric particle (one shell corresponding to the

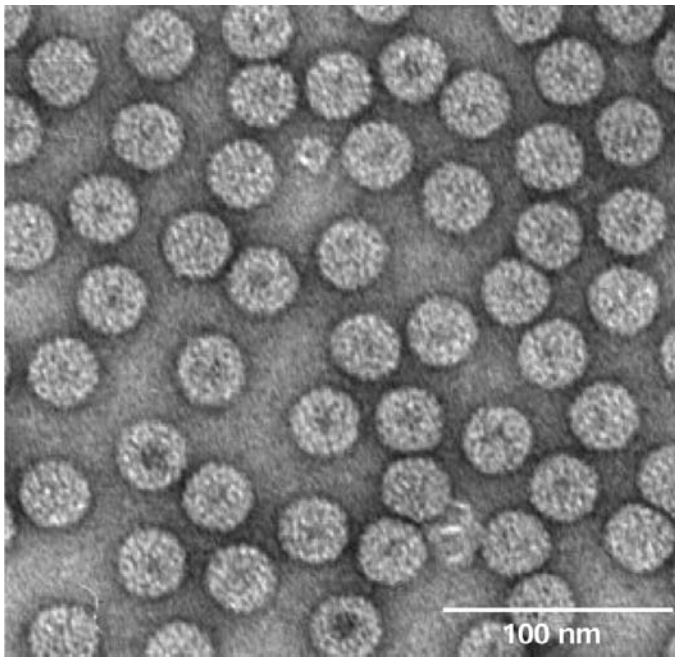

Figure 1
Electron micrograph of a 250 μg ml^{-1} BMV solution negatively stained with 1%(*w*/*v*) uranyl acetate solution at pH 4.

protein, the second shell to protein and solvent, the third shell to protein and RNA and the last two corresponding to a progressive decrease of RNA density). Image reconstruction has shown that the surface of BMV presents the same capsomer organization (hexamers and pentamers) as cowpea chlorotic mottle virus (CCMV), another bromovirus, the structure of which has already been determined at 3.2 Å resolution (Speir *et al.*, 1995). Moreover, the BMV capsid protein presents 70% sequence identity with the capsid protein of the CCMV (SwissProt accession No. P03601). Neither the RNA nor the N-terminal regions of the coat protein are ordered at high resolution, but it is known that their interaction is essential for the morphogenesis and the stability of the virions (Chidlow & Tremaine, 1971; Cuillel *et al.*, 1981; Speir *et al.*, 1995). To obtain additional information about the icosahedral viruses, we undertook completion of the studies on BMV by determining its structure at high resolution by crystallization and X-ray diffraction.

X-ray crystallography is the only way to determine the three-dimensional structures of very large macromolecules at high resolution. The limiting stage is to obtain crystals, which is generally possible for proteins under attractive interaction conditions (Ducruix *et al.*, 1996; George & Wilson, 1994; Muschol & Rosenberger, 1995; Tardieu *et al.*, 2001). Although various spherical plant viruses have already been crystallized, no systematic recipe was established, as the various viruses were crystallized under very different conditions of concentration, pH and precipitant types.

Until now, little has been known about interactions between isometric virions in solution, except that neutron-scattering studies have shown that these viruses generally present repulsive interactions at physiological pH and ionic strength, and behave like monodisperse solutions. In a systematic study of crystallization conditions, we investigated the interactions between BMV particles in solution under various experimental conditions in order to find out the conditions under which interactions become attractive. Studies of interactions between macromolecules in solution, using techniques such as osmotic pressure, light scattering and small-angle X-ray scattering (SAXS), have already been described for various globular soluble proteins, ranging from bovine pancreatic trypsin inhibitor (6.5 kDa; Lafont *et al.*, 1997) to α-crystallins (800 kDa; Finet, 1999; Finet & Tardieu, 2001), and including lysozyme (14.3 kDa; Bonneté *et al.*, 1999; George & Wilson, 1994; Muschol & Rosenberger, 1995; Tardieu *et al.*, 1999), ribonuclease A (15.7 kDa; Boyer *et al.*, 1999), γ-crystallins (21 kDa; Bonneté *et al.*, 1997; Finet, 1999; Malfois *et al.*, 1996), chymotrypsinogen (25.7 kDa; Velev *et al.*, 1998), urate oxidase (128 kDa; Bonneté *et al.*, 2001), ATCase (306 kDa; Budayova *et al.*, 1999) and apoferritin (450 kDa; Petsev & Vekilov, 2000). These studies provided much information about the behaviour of proteins in solution with regard to attractive and repulsive interactions for particles of mass lower than 800 kDa. Our work on BMV particles therefore extends this kind of study to the realm of very large supramolecular assemblies.

Interactions between macromolecules in solution are driven by different forces that include colloidal forces, *i.e.* hard-sphere, van der Waals, electrostatic and depletion forces (Israelachvili, 1994, Poon *et al.*, 1996). Hard-sphere interactions are repulsive: they express the fact that macromolecules cannot interpenetrate. The van der Waals interactions act like a short-range attractive potential with small proteins in solution (Israelachvili, 1994), but become negligible with large macromolecules. The main electrostatic force is the coulombian repulsion, which depends upon charge and ionic strength. These three forces are included in the DLVO potential (Derjaguin–Landau–Verwey–Overbeek; Derjaguin, 1940; Israelachvili, 1994; Verwey *et al.*, 1948). With proteins, other contributions play a role in addition to colloidal forces. For instance, it has been shown for many proteins (Bonneté *et al.*, 1999; Budayova *et al.*, 1999; Finet, 1999; Muschol & Rosenberger, 1995; Tardieu *et al.*, 1999) that the addition of monovalent salts not only screens the particle charges, but induces an additional attraction. The attraction varies according to the nature of the anions, following the reverse order of the Hofmeister series (Hofmeister, 1888) when the protein is studied at a pH below its isoelectric point pI and the direct Hofmeister order above the pI. An easy-to-use coefficient to characterize the interactions in solution is the second virial coefficient (Bonneté *et al.*, 1999; George & Wilson, 1994; Guo *et al.*, 1999; Haas *et al.*, 1999; Lafont *et al.*, 1997; Muschol & Rosenberger, 1995; Veesler *et al.*, 1996; Velev *et al.*, 1998), whose sign indicates the nature of the interactions, repulsive or attractive (see §2).

Depletion forces may be induced by the addition of polymers such as PEG into the solution; their range is a function of the polymer size and conformation (Asakura & Oosawa, 1958; Poon *et al.*, 1996; Ye *et al.*, 1996). When the distance between neighbouring particles is smaller than the polymer diameter,

the polymers are excluded from the region between the particles. To maximize the translation entropy of polymers, this inaccessible volume is minimized by driving the virus particles close to one another, thereby introducing an additional attractive force between viruses. With protein solutions, the attractive contribution associated with PEG is a function of PEG concentration and molecular weight (Bonneté *et al.*, 2001; Budayova *et al.*, 1999; Finet & Tardieu, 2001; Kulkarni *et al.*, 2000).

On the basis of all of these previous studies made on macromolecules, we have used SAXS to study the evolution of interactions between BMV particles as a function of pH and salt or polymer type and concentration, and to finally establish crystallization conditions.

2. Materials and methods

2.1. BMV preparation

10 d old barley seedlings were inoculated with a 100 µg ml^{-1} BMV solution containing abrasive powder (Carborundum 600, Avocado). The barley leaves were crushed 15 d later in 20 m*M* sodium acetate buffer pH 5.9; the pH was then adjusted to pH 4.8 with acetic acid to induce the precipitation of the plant proteins (Bockstahler & Kaesberg, 1962) and left at 277 K for 2 h. The viruses were isolated by two cycles of differential centrifugation at 8000 rev min^{-1} (at 285 K for 15 min) and 45 000 rev min^{-1} (at 285 K for 90 min). Finally, purified viruses were filtered through 0.45 and 0.2 µm filters (Pfeiffer & Hirth, 1974) and stored at 277 K and pH 5.9 in a 20 m*M* sodium acetate buffer. The yield of the purification was of about 150 mg of BMV per 100 g of barley leaves. The final concentration was determined by optical density measurement at 260 nm (ε = 5.08 mg ml^{-1} cm^{-1}).

For X-ray experiments, the pH of the viral solutions was adjusted to the desired value with acetic or hydrochloric acid or NaOH. $CaCl_2$ at a final concentration of 3 m*M* was added to the pH 7.5 buffer in order to prevent virus swelling at this pH (Perez *et al.*, 2000).

2.2. Electron microscopy

The BMV solution diluted to 0.25 mg ml^{-1} was adsorbed for 1 min onto a 200 mesh grid covered with a carbon film and after blotting was negatively stained for 2 min with a 1%(*w*/*v*) aqueous uranyl acetate solution at pH 4. The preparation was photographed with a Philips EM 201 transmission electron microscope at ×45 000 magnification.

2.3. Small-angle X-ray scattering (SAXS) experiments in solution

The intensity scattered by one particle as a function of the scattering vector diffractometer **s** (with $s = 2\sin\theta/\lambda$, where λ is the wavelength and 2θ is the scattering angle) is usually called the particle form factor and corresponds to the Fourier transform of the spherically averaged autocorrelation function of the electron-density contrast of the particle (Luzzati & Tardieu, 1980). When the solution is ideal, that is to say in the absence of interactions, the total scattering coincides with $I(s)$, the form factor of the particle. With solutions of monodisperse spherical particles and in the presence of interactions, departure from ideality may simply be accounted for by a dependence of the scattered intensity on concentration. In this case, the scattered intensity $I(c, s)$ can be expressed as a product of $I(s)$ with an interference factor, $S(c, s)$, called the solution structure factor,

$$I(c, s) = I(s) \cdot S(c, s). \quad (1)$$

$S(c, s)$ is the Fourier transform of the autocorrelation of the distribution of the particles and thus reflects the interactions between particles. With repulsive interactions, the particles are evenly distributed and the intensity at zero angle decreases as particle concentrations increase. With attractive interactions, fluctuations in the particle distribution are observed which lead to an increase of $I(c, 0)$ with the increase in concentration. Note that the form factor $I(s)$ of the particle can be obtained by extrapolating experimental data to $I(0, s)$. The relation (1) can be written as follows (Tardieu, 1994),

$$I(c, s) = I(0, s) \cdot S(c, s). \quad (2)$$

The experiments were carried out using the small-angle instrument D24 using the synchrotron radiation emitted by the storage ring DCI at the Laboratory for Synchrotron Radiation, LURE (Orsay). Data were collected using a linear position-sensitive detector with delay line readout. The sample-to-detector distance was 2.641 m, except for the determination of the form factor where it was 1.891 m, yielding an *s*-increment per channel of 0.15395×10^{-3} and 0.21359×10^{-3} Å^{-1}, respectively. The average recorded *s* range was $1 \times 10^{-3} < s < 4.5 \times 10^{-2}$ Å^{-1}. The wavelength of the X-rays was 1.488 Å (*K* edge of Ni). The experiments in solution were performed with a specially designed quartz cell operated under vacuum (Dubuisson *et al.*, 1997) that could be filled and rinsed *in situ*. Several successive frames were recorded for each sample and for the corresponding buffer. The total exposure time was 30 s for a 40 mg ml^{-1} virus solution, 60 s for a 20 mg ml^{-1} solution, 120 s for a 10 mg ml^{-1} solution and 240 s for a 5 mg ml^{-1} solution. The samples were obtained by successive dilutions of the 40 mg ml^{-1} sample with a buffer containing the same precipitating agent concentrations. The curves were scaled to the transmitted intensity and averaged when no radiation damage was observed. The scattered intensity curves, $I(c, s)$, were subtracted for background and, within each series, properly normalized: for concentration series data were divided by the virus concentration, while for series at constant virus concentration data were normalized at constant $I(0,0)$.

2.4. SAXS data treatment

2.4.1. Determination of the form factor. The form factor of the BMV was first determined at pH 5.9 in its storage buffer (20 m*M* sodium acetate). The low-angle and the medium-angle part of the form factor of the virus were recorded separately using two different samples and two detector distances. At low angles, measured at 2.641 m ($0.001 < s <$

0.009 Å^{-1}), a concentration series from 40 to 5 mg ml^{-1} BMV was recorded and the curves extrapolated to infinite dilution corresponding to scattering by ideal solution. At larger angles, at a distance of 1.891 m ($0.009 < s < 0.02$ Å^{-1}), where the interactions are negligible, we recorded a 40 mg ml^{-1} BMV spectrum in order to obtain a better signal-to-noise ratio in this region.

2.4.2. Extrapolation. To obtain the form factors, that is to say the intensity scattered by a unique particle, corresponding to each pH or salt condition, we calculated the values of $1/I(c, s)$ for each of the 16 first values of s, corresponding to the channels 7–22 closest to the origin (the seven first channels were not usable because of the beamstop). We only used the intensities corresponding to the 5 and 10 mg ml^{-1} BMV solutions, because there were too strong effects at concentrated solutions. These values were then used to plot $1/I(c, s) = f(c)$ curves. The linear fit of this Zimm plot permitted us to obtain the $I(0, s)$ values for each s value. I$(0, s)$ values were then used in Guinier plots, *i.e.* plots of $\ln I(0, s)$ *versus* s^2, which permitted us to determine the $I(0, 0)$ values according to the Guinier law,

$$I(0, s) = I(0, 0)\exp[-(4/3)\pi^2 R_g^2 s^2], \quad (3)$$

where R_g is the radius of gyration of the particle. For each condition, the combination of the values $I(0, 0)$ of the extrapolation with the 16 $I(0, s)$ values, completed with the 40 mg ml^{-1} data, permitted us to obtain the form factors. The missing values of $I(0, s)$ corresponding to $s < 1.10$–3 Å^{-1} were extrapolated according to (3).

2.4.3. Spherical models. Virions are modelled as hollow spheres with external and internal radii. The experimental curves $I(c, s)$ were compared with theoretical ones $I(s)_{\rm theo}$ corresponding to the scattered intensity of hollow spheres whose external ($R_{\rm ext}$) and internal ($R_{\rm int}$) radii values were varied. The best fit was determined as a function of the alignment of the two first intensity minima and as a function of the superposition of the two first secondary maxima.

We used the Fourier transform of a solid sphere of radius R,

$$F(s) = 3F(0)(\sin u - u\cos u)/u^3, \quad (4)$$

where $F(0)$ is equal to $(4/3)\pi R^3\rho$, ρ is the uniform electron density of the sphere and u is equal to $2\pi Rs$. The scattered intensity curve of a hollow sphere would then correspond to

$$I(s)_{\rm theo} = [F_{\rm ext}(s) - F_{\rm int}(s)]^2, \quad (5)$$

where $F_{\rm ext}(s)$ corresponds to a sphere of radius $R_{\rm ext}$ and $F_{\rm int}(s)$ corresponds to a sphere of radius $R_{\rm int}$.

2.4.4. Patterson models. The distributions of the distances r between scattering atoms were computed with the *GNOM* program, written by Svergun & Semenyuk (1993) (Feigin & Svergun, 1987), that evaluates the distance-distribution function $p(r)$ for monodisperse systems from the experimental scattering data

$$p(r) = r^2 \cdot P(r), \quad (6)$$

where r is the distance between two atoms and $P(r)$ is the Patterson function related to $I(s)$ by

$$P(r) = \frac{2}{r}\int s \cdot I(s)\sin(2\pi rs)\,{\rm d}s.$$

2.4.5. Second virial coefficient A_2. Under the influence of repulsive interactions the distribution of the macromolecules is relatively uniform in solution, while with attractive interactions strong fluctuations of distribution may occur. Without interactions, the osmotic pressure can be written as $\Pi = \rho kT$, where ρ is the particle density, k is the Boltzmann constant and T the absolute temperature. In the case of interactions in solution, the osmotic pressure can be expanded in a power series of ρ,

$$\Pi/\rho kT = 1 + B_2\rho + B_3\rho^2 + \ldots \quad (8)$$

where B_2 is the second virial coefficient. The sign of B_2 gives direct information about the type of interactions involved: B_2 is negative with attractive interactions and positive with repulsive ones. In practice, ρ is converted into the macromolecular concentration c in g cm^{-3} using $\rho/N_{\rm A} = c/M$, where M is the molecular weight in daltons and $N_{\rm A}$ is Avogadro's number, to yield

$$\Pi/cRT = 1 + A_2c + A_3c^2 + \ldots, \quad (9)$$

where R is the gas constant and $A_2 = B_2N_{\rm A}/M^2$. The X-ray structure factor at the origin gives access to A_2, as it is related to the osmotic pressure by the following expressions,

$$S(c, 0) = (RT/M)(\partial\Pi/\partial c)^{-1}, \quad (10)$$

$$1/S(c, 0) = 1 + 2MA_2c = 1 + 2B_2\rho. \quad (11)$$

2.4.6. Indexation of the diffraction peaks. The position of the diffraction peaks is inversely proportional to the repetition distance d between equivalent planes in the crystal. In the case of a crystal where the three angles α, β and γ of the cell are equal to 90°, as is the case for cubic and orthorhombic systems, we have

$$s = \frac{1}{d} = \left(\frac{h^2}{a^2} + \frac{k^2}{b^2} + \frac{l^2}{c^2}\right), \quad (12)$$

where a, b and c are the dimensions of the crystalline cell and h, k and l are the Miller indices of the planes. [For the permitted reflections of the cubic and orthorhombic systems see *International Tables for X-ray Crystallography* (1952).]

2.5. Microbatch experiments

The experiments were undertaken with BMV concentrations ranging from 5 to 40 mg ml^{-1}. The virus was mixed with PEG 8000 or PEG 20 000 from 3 to 10%(*w*/*v*). The drops were set down in microbatch plates, covered with paraffin oil to avoid evaporation and stored at 293 K. The samples were photographed each day with a TSE Microscope at ×4 magnification (visualized and recorded on a Microvision system at ×2.5 magnification).

3. Results

3.1. SAXS studies as a function of pH

Varying pH changes interactions between macromolecules by modifying the net charge of the particles and therefore the coulombian repulsion. The following pH values were used: 4.0, 5.0, 5.9 and 7.5 at low ionic strength (20 m*M* sodium acetate). In order to prevent the swelling of BMV at pH 7.5, the latter buffer also contained 5 m*M* $CaCl_2$. Under our SAXS experimental conditions, the accessible range of concentrations able to guarantee optimal conditions was 40–5 mg ml^{-1} BMV. This range permitted us to determine the form factor of the virus using the lowest concentration and to observe the interactions in solution with the highest concentration without requiring too much material.

3.1.1. Form factor. The form factor of the BMV in its storage buffer (20 m*M* sodium acetate pH 5.9) was determined by superposing the low-angle part obtained by extrapolating the curve at 5 mg ml^{-1}, where the interactions are almost negligible, and the medium-angle part of the data obtained at higher BMV concentration, where the signal-to-noise ratio is the highest (see §2). As can be seen in Fig. 2(*a*), the X-ray spectrum of the form factor presents at low angles a succession of lobes with minima and maxima characteristic of the scattering of a monodisperse solution of spherical particles, whereas at higher angles the contribution arising from the icosahedral symmetry of the capsid shows up. In the following experiments, only the low-angle part of the scattering curves was recorded, since the contribution of the interactions between particles is particularly visible in the region near the origin, which we will call the 'interaction zone'.

Previous neutron-scattering studies showed that BMV displays several protein and/or RNA shells and a central hole (Jacrot *et al.*, 1977; Zulauf *et al.*, 1983). With neutrons, a detailed description of the BMV structure is possible, as the protein and the RNA do not have the same contrast and can thus be distinguished. Conversely, with X-rays, the protein and the hydrated RNA have the same contrast; therefore, it is not possible to separate the contribution of the two components and the measured scattering can only give access to the radial distribution of matter (protein or RNA) with respect to the solvent. In the case of BMV, a homogeneous spherical shell accounts very well for the inner part of the scattering curve ($s < 0.01$ Å^{-1}). We used such a model, which we call a 'hollow-sphere model'. The external and internal radii were determined for each pH condition by fitting our experimental curve with this model (see §2).

Fig. 2(*b*) represents the experimental data obtained at pH 4, 5, 5.9 and 7.5 at 40 mg ml^{-1} BMV concentration. A slight shift of the minima positions and a variation of the height of the first secondary maxima associated with pH increase can be observed, revealing a structural modification of the virus. These experimental data were extrapolated to infinite dilution to obtain the corresponding form factors. We fitted the curves with 'hollow-sphere models'. The internal and the external radii of the models were varied in each case and the best fit parameters are given in Table 1, the corresponding curves being shown in Fig. 3(*a*). Table 1 shows that the internal radius is the only parameter that decreases with the increase of the

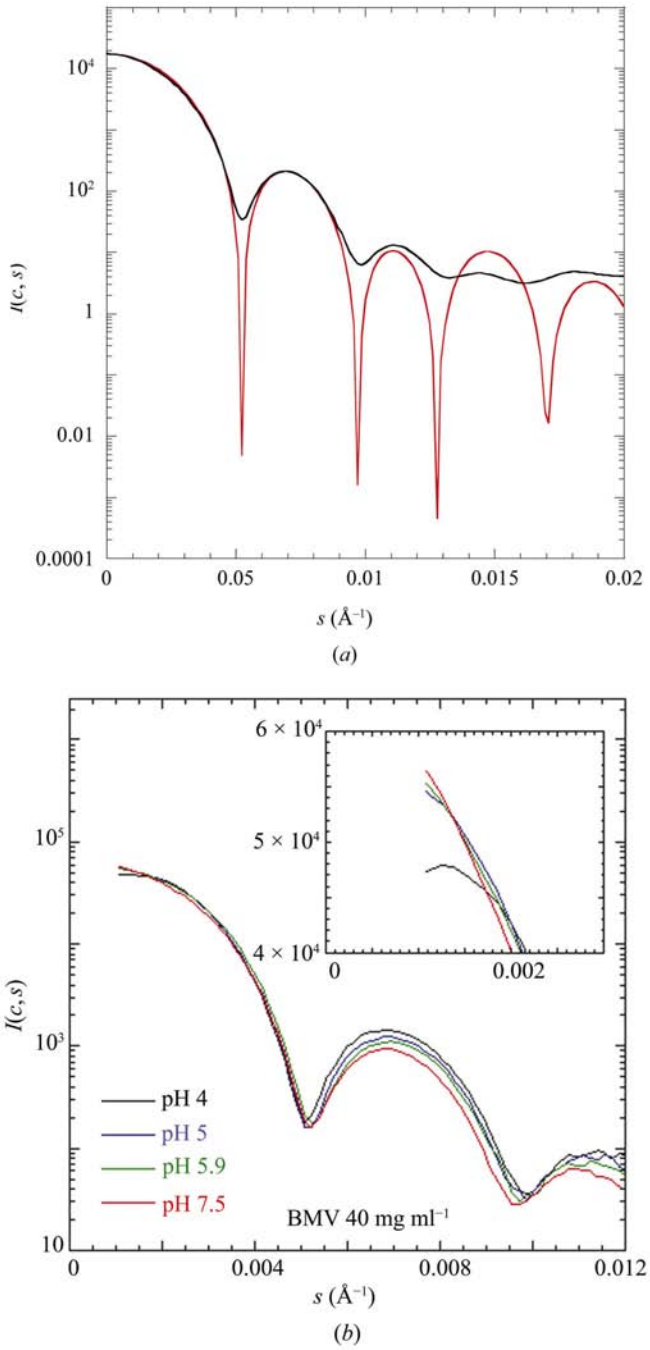

Figure 2
Small-angle scattering curves of BMV in solution in 20 m*M* sodium acetate buffer at different pH values; the scattered intensity $I(c, s)$ is plotted against $s = 2\sin\theta/\lambda$, where 2θ is the scattering angle and λ is the wavelength of the X-rays. (*a*) Black line, form factor of the BMV at pH 5.9, obtained by combining low-angle scattering data from a 5 mg ml^{-1} solution with medium-angle scattering data from a 40 mg ml^{-1} solution. Red line, simulated scattering data of the hollow-sphere model: the best fit was obtained with R_{ext} = 132 Å and R_{int} = 40.5 Å. (*b*) Normalized scattering data at different pH values: 4, 5, 5.9, 7.5; insert: enlargement of the 'interaction zone' (see text).

Table 1
R_{ext} and R_{int}.

R_{ext} and R_{int} values were determined with the hollow-sphere models for each condition of pH and $NaNO_3$ concentration.

	R_{ext} (Å)	R_{int} (Å)
pH 4	131	52
pH 5	132	46
pH 5.9	132	40.5
pH 7.5	133	39
0.1 *M* $NaNO_3$	132	48
0.2 *M* $NaNO_3$	131	46
0.5 *M* $NaNO_3$	132	34

Table 2
A_2M values.

A_2M values calculated for each conditions of pH value, $NaNO_3$ concentration or PEG 8000 percentage (*w*/*v*), where the molecular weight $M = 4.6 \times 10^6$ Da. Crystallization of BMV occurs as soon as the A_2 value becomes close to 0. Noteworthy is the fact that one slightly negative A_2 value was found in the case of the satellite tobacco mosaic virus ($T = 1$) (Malkin & McPherson, 1993).

pH value	A_2M	$NaNO_3$ concentration (*M*) (pH 4)	A_2M	PEG 8000 [%(*w*/*v*)] (pH 5)	A_2M
4	9.2	0	9.2	0	5.8
5	5.8	0.1	4.3	4	4.4
5.9	6.3	0.2	2.1	6	3.5
7.5	3.3	0.5	2.8	8	1.2

pH, whereas the outer radius remains constant, providing evidence for a reorganization (swelling) of the RNA.

The distributions of the distances *r* between the scattering atoms (Feigin & Svergun, 1987; Svergun & Semenyuk, 1993) (Fig. 3*b*) confirms that only the diameter of the hole varies with pH, since the maxima of the distributions are shifted towards small *r* values with the increase of pH, whereas the outer diameter remained constant at 264 ± 2 Å. Indeed, $P(r)$ curves calculated for the spherical shell models reproduced the experimentally observed variations (data not shown).

3.1.2. Interactions. For each pH value, the X-ray scattering patterns were recorded for a decreasing BMV concentration series, obtained by successive dilutions from 40 to 5 mg ml^{-1}. The results obtained at pH 5.9 are shown in Fig. 4(*a*); the insert shows that there is no variation of the first minimum or of the first secondary maximum of the curves as a function of the concentration at constant pH value. The intensity near the origin decreases as the virus concentration increases, which means that the interactions are repulsive.

In the pH range explored (pH 4–7.5), the interactions between the viruses in solution remain repulsive, although the scattering curves indicate a progressive decrease of the repulsive interactions with the increase of pH from 4 to 7.5 (see insert, Fig. 2*b*). The decrease of the second virial coefficient, A_2, with increasing pH confirms the decrease in these repulsive interactions (Fig. 4*b* and Table 2).

3.2. Effect of the addition of salt

Since a variation of pH has been shown to result in a structural reorganization of the BMV as well as in a modifi-

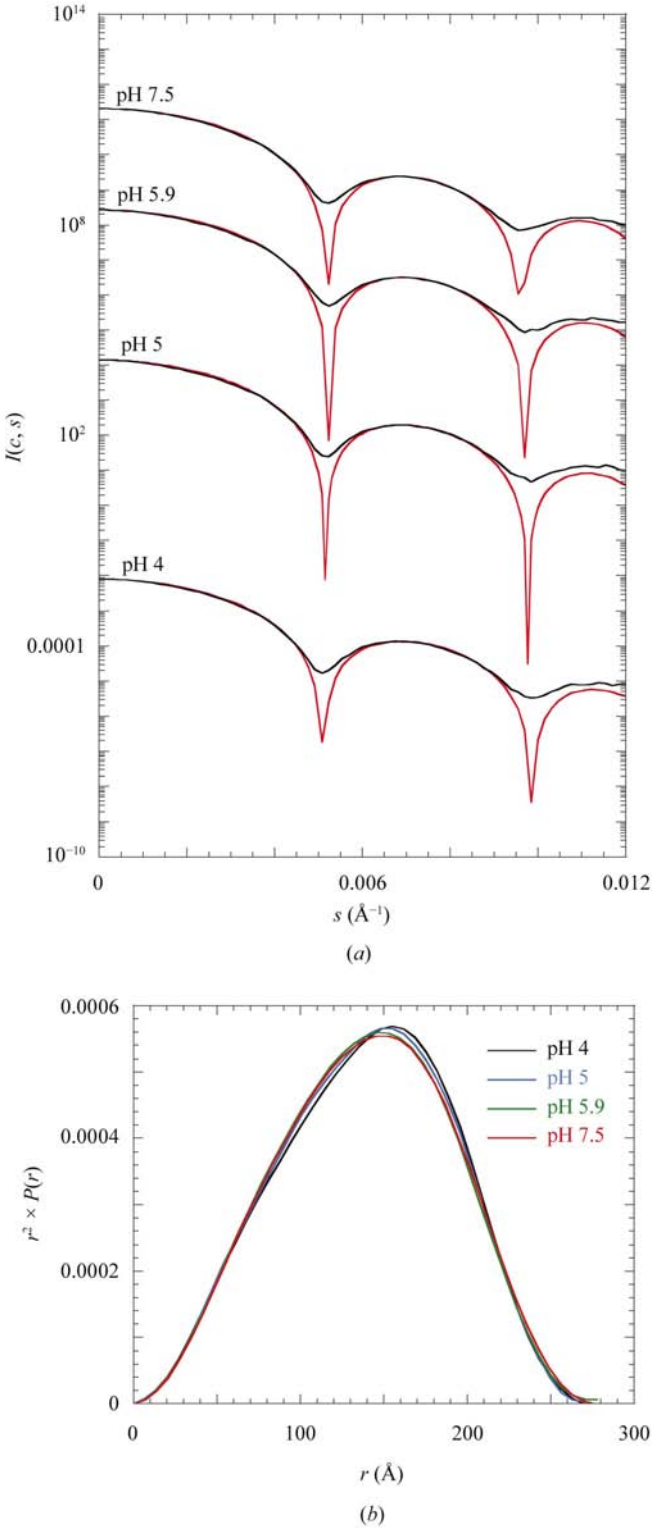

Figure 3
Characterization of the effects of pH variation. (*a*) Superposition of the extrapolated experimental curves obtained at pH 4, 5, 5.9 and 7.5 and the best fit hollow-sphere models obtained by varying the internal and the external radii. For the sake of clarity, curves corresponding to each pH value were shifted with respect to each other. (*b*) Distributions of the distances *r* between scattering atoms at pH 4, 5, 5.9 and 7.5. Note the progressive shift with pH of these distributions towards the low *r* values that indicates a progressive filling of the central hole.

cation of the interactions in solution, we took care to compare the effect of different salts and concentrations of salts at constant pH values. We chose to work at pH 4, because at this pH the repulsion at low salt is highest and moreover the virions are the most compact and thus stable.

3.2.1. Form factor. The analysis of the data obtained with two different salts, sodium acetate and $NaNO_3$, reveals a shift of position of the first minimum towards larger angles in presence of 0.2 *M* $NaNO_3$ which did not occur with the same concentration of sodium acetate (Fig. 5*a*). To analyze this variation, we used a series of concentration of $NaNO_3$ for concentrations of BMV from 40 to 5 mg ml^{-1}. The results obtained with 40 mg ml^{-1} virus solutions in the presence of 0.1, 0.3 and 0.5 *M* $NaNO_3$ are shown in Fig. 5(*b*). A noticeable shift of the first minimum positions and a variation of the height of the first secondary maximum according to the increase in $NaNO_3$ concentration reveal a progressive modification of the internal organization of the virion. Fitting the curves with a 'hollow-sphere model' and calculating the distributions of the distances *r* between the scattering atoms (Figs. 6*a* and 6*b*, respectively) showed that there was a progressive decrease of the internal radius of the virus with the increase in $NaNO_3$ concentration (Table 1), while the external radius remained unchanged, indicating a progressive reorganization of the RNA as a function of salt concentration.

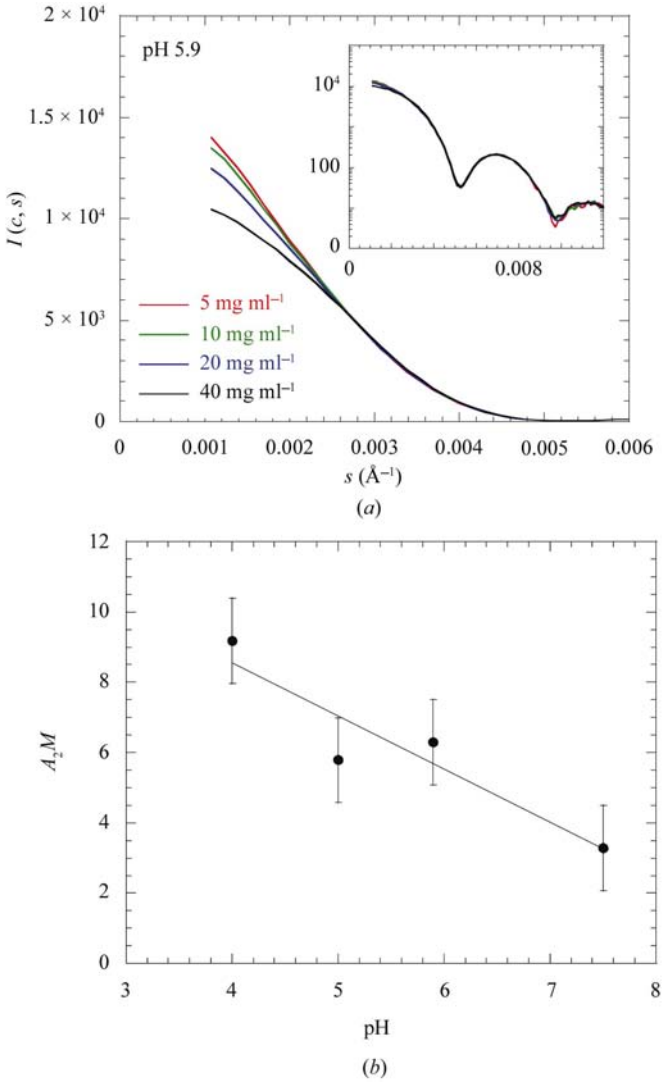

Figure 4
(*a*) Normalized scattered intensities of BMV from 5 to 40 mg ml^{-1} concentration at pH 5.9 (insert: log representation of the scattering curves showing the interaction zone, which is bounded by the first intensity minimum). (*b*) Variation of the second virial coefficient A_2 as a function of pH, showing that interactions are less repulsive at higher pH (the molecular weight $M = 4.6 \times 10^6$ Da).

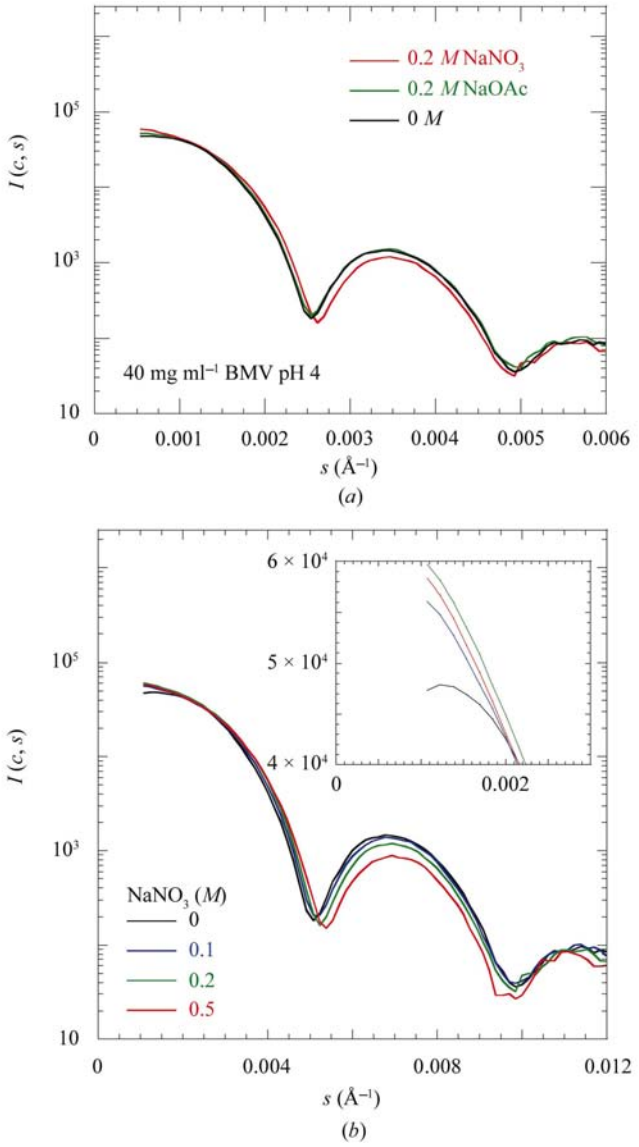

Figure 5
Characterization of the effects of salt type and concentration: comparison of the effect of $NaNO_3$ and sodium acetate at 0.2 *M*. The repulsive interactions decrease in a more visible way with $NaNO_3$ than with sodium acetate; a structural change is observed with the use of $NaNO_3$, as revealed by the shift of the first intensity minimum and the variation of the height of the first secondary maximum. (*a*) Progressive structural change of the virus with the increase of $NaNO_3$ concentration from 0 to 0.5 *M*. (*b*) Insert: enlargement of the interaction zone. 0.5 *M* $NaNO_3$ is not more efficient than 0.2 *M* in reducing the repulsive interactions.

3.2.2. Interactions. The effects of 0.2 *M* $NaNO_3$ were first compared with those of 0.2 *M* sodium acetate (Fig. 5*a*). With proteins, the Hofmeister effect follows the inverse order of the Hofmeister series when pH < pI. Sodium acetate is at one end of the series and $NaNO_3$ at the other end. Both salts were found to be efficient in reducing the repulsive interactions, but the influence of $NaNO_3$ was found to be stronger. However, even at the highest concentration used, 0.5 *M*, this salt does not lead to attractive interactions. The screening of the charges at high concentrations of $NaNO_3$ is confirmed by the observation that the second virial coefficient does not change upon increasing the $NaNO_3$ concentration from 0.2 to 0.5 *M* (Fig. 6*c* and Table 2).

3.3. Combination of the effects of the salts with PEG

Since the combination of salt and PEG had already been observed to result in a synergetic increase of the attractive interactions of proteins (Atha & Ingham, 1981; Bonneté *et al.*, 2001; Budayova *et al.*, 1999; Finet & Tardieu, 2001), we explored such conditions on a larger particle, BMV. Adding 5%(*w*/*v*) PEG 20 000 to a sample containing 0.1 *M* $NaNO_3$ led to immediate precipitation. The effect of sodium acetate (0.1–0.3 *M*) in the presence of 5%(*w*/*v*) PEG 20 000 is shown in Fig. 7(*a*). Precipitation, implying strong attraction, occurred in the BMV samples containing 0.2 *M* sodium acetate and 20 mg ml^{-1} BMV or more and for all the samples containing 0.3 *M* sodium acetate. The synergetic effect between salt and PEG is clearly visible in Fig. 7(*b*): while with 0.2 *M* sodium acetate alone the interactions in a 40 mg ml^{-1} BMV solution remain repulsive, the same amount of salt produces an immediate precipitate in presence of 5%(*w*/*v*) PEG 20 000. Notably, the X-ray spectra recorded to check the macroscopic structure of the precipitates always produced diffraction peaks, indicating that the precipitates are microcrystalline and not amorphous. Moreover, this observation indicated that we had reached crystallization zones.

3.4. Characterization of interactions in presence of PEG

Since precipitation occurred with the combined use of salt and PEG, the effects of the progressive addition of polymers to low-salt (20 m*M* sodium acetate) buffers were studied in more detail to find out if attractive conditions could be reached with PEG alone. At pH 5.9, the 40 mg ml^{-1} BMV sample precipitated in presence of 4%(*w*/*v*) PEG 20 000 and gave rise to diffraction peaks. The solution was still turbid after the dilution of BMV concentration at 20 mg ml^{-1}, where peaks started to emerge (Fig. 8*a*). To avoid this too strongly attractive effect of PEG, another PEG, PEG 8000, was used at pH 5. We varied its concentration from 4 to 8%(*w*/*v*), since neither precipitate nor turbidity appeared at 4%(*w*/*v*) PEG 8000 in the presence of 40 mg ml^{-1} BMV (Fig. 8*b*). The interaction regime seems to become attractive with 8%(*w*/*v*) PEG 8000 at pH 5.

The representation of the second virial coefficient A_2, shown in Fig. 8(*c*), as a function of PEG 8000 concentration in non-precipitating conditions confirms that PEG adds an attractive factor in solution. A_2M values are reported in Table 2.

At low virus and/or PEG 8000 or 20 000 concentrations, the samples were clear and no pellet was observed at low-speed centrifugation. At high concentration of virus and/or PEG, a precipitation was observed and a low-speed centrifugation permitted the isolation of two phases, a translucent phase corresponding to the buffer and PEG and another, completely opaque, phase containing the virions. At pH 5, precipitation occurred at 10%(*w*/*v*) PEG 8000 for all BMV concentrations (insert in Fig. 8*b*) and diffraction peaks were observed. Precipitation occurs therefore with PEG as soon as an attraction threshold is reached.

3.5. Diffraction peaks

All the precipitates obtained were made of microcrystals. That was unambiguously revealed by the immediate appearance of diffraction peaks observed not only in precipitated samples but also in merely turbid samples. Fig. 9 describes the aspect of the samples that were studied by SAXS immediately after mixing the different components. In the turbid samples, the microcrystals were in equilibrium with viruses in solution. These results indicated that the phase separation induced by PEG was similar to a liquid–solid phase separation and allowed us to determine the precipitation zones.

In all conditions leading to microcrystals, these were formed rapidly since the diffraction peaks were already present at the end of the 2 min required after mixing to start the X-ray experiments. Moreover, the positions of the Bragg peaks were conserved, which indicated that the crystal cell remained the same in all experiments. The spacing of the reflections (insert, Fig. 8*b*) were close to the following ratio: $2^{1/2}$, $6^{1/2}$, $8^{1/2}$, $14^{1/2}$ and $16^{1/2}$, which could account for a centered cubic system, with a lattice size of about 330 Å, consistent with the fact that icosahedral viruses crystallize in cubic, hexagonal or orthorhombic systems, owing to their spherical shape. However, since the peaks were not exactly following the ratio expected with a cubic lattice, it is probable that the lattice is in fact orthorhombic. The microcrystalline phase looks stable and was not observed to evolve into larger crystals over a period of two months.

3.6. Phase diagrams in the presence of PEG

Since SAXS experiments provided us with several crystallization conditions, we could predict that larger crystals would be obtained in conditions slightly less concentrated in PEG than the conditions which yielded microcrystals. This exploration of the phase diagram was performed using batch experiments.

The phase diagrams of BMV concentration as a function of percentage of PEG 8000 (pH 5) and PEG 20 000 (pH 5.9), obtained with microbatch experiments, are represented in Fig. 10. The protein concentration was varied from 5 to 40 mg ml^{-1} and the PEG concentration from 3 to 10%(*w*/*v*). During the preparation, soluble, turbid and precipitated samples were reproducibly obtained in the same conditions as

for the SAXS experiments. [No evolution of the SAXS precipitates was observed as a function of time (over one month).] Data points in Fig. 10 represent the aspect of the microbatch wells after a week. Solubility-like curves were added to guide the eye. In the case of the samples corresponding to the turbid SAXS samples, ill-shaped crystals were observed to emerge after a week. 2 d after the beginning of the experiment, we could observe the growth of well isolated small crystals from transparent samples, as shown in Fig. 10, in solutions that were close to the precipitation limit in the case of PEG 20 000. In fact, as soon as the virus concentration is higher than 10 mg ml^{-1} (Fig. 10*a*), solutions containing even a small percentage of PEG 20 000 had a precipitated aspect, known to be microcrystalline, which restricted the macrocrystallization conditions; however, all these conditions led to a fast formation of small crystals (in a couple of days). With PEG 8000, the limit of the solubility curve varied much more with the virus concentration, from 5 to 30 mg ml^{-1} BMV in presence of 8 to 3%(*w*/*v*) PEG 8000 (Fig. 10*b*), but the small crystals appeared much later (about 4 d).

4. Discussion

4.1. Structural characterization of the BMV

In this study, the existence of a central hole in the BMV was confirmed by SAXS experiments, since a good fit could be obtained with a hollow-sphere model (Fig. 2*a*).

The changes of pH from 4 to 7.5 were found to modify the virus structure slightly, as revealed by a shift of the minima and by a variation of the height of the first secondary maximum of the scattering curves (Fig. 2*b*). Hollow-sphere models show

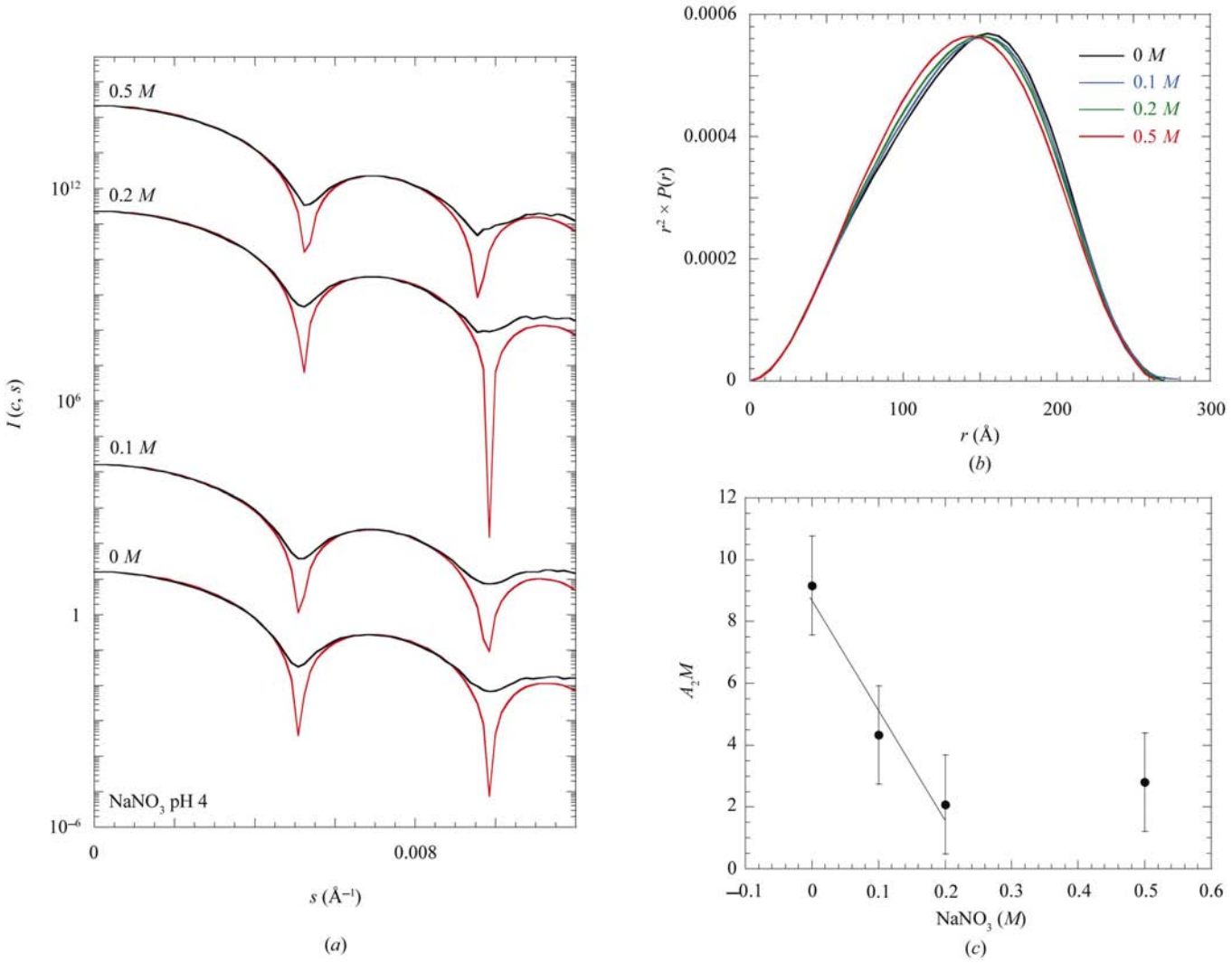

Figure 6
Characterization of the effects of $NaNO_3$. (*a*) Superposition of the extrapolated experimental curves obtained by changing $NaNO_3$ concentration and the best-fit hollow-sphere models obtained by varying the internal and the external radii. For the sake of clarity, curves corresponding to each $NaNO_3$ concentration were shifted with respect to each other. (*b*) Distributions of the distances *r* between scattering atoms corresponding to 0, 0.1, 0.2 and 0.5 *M* $NaNO_3$. There is a progressive shift of these distributions towards the low *r* values, indicating a progressive filling of the central hole. (*c*) Decrease of the second virial coefficient A_2 as a function of $NaNO_3$ concentration, showing that the interactions become less repulsive (molecular weight $M = 4.6 \times 10^6$ Da).

that these variations may be attributed to a modification of the RNA volume occupancy, as the internal diameter decreases with the increase of pH value (Table 1, Fig. 3*a*). The outer diameter remains constant, 264 ± 2 Å, whereas the internal radius undergoes a reduction of 25% upon varying the pH from 4 to 7.5. Considering that at acidic pH the outer radius of

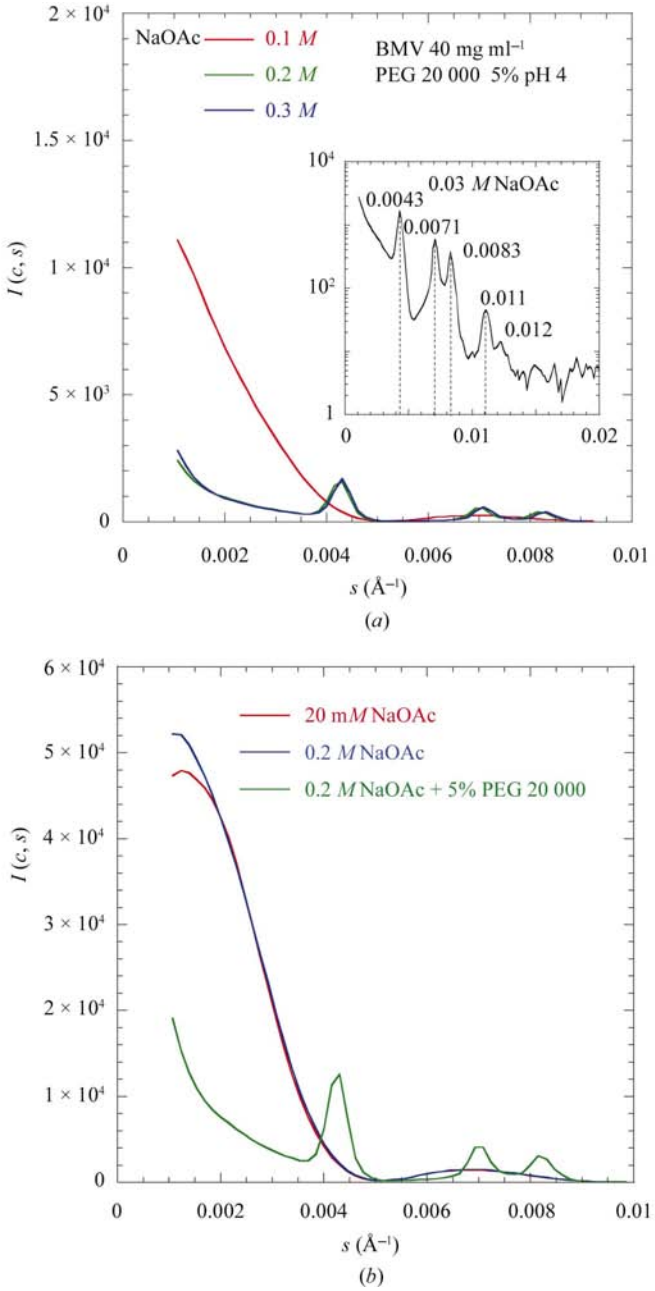

Figure 7
Synergetic effect of PEG 20 000 and salt. (*a*) Effect of the combination of 5%(*w*/*v*) PEG 20 000 with 0.1 *M*, 0.2 *M* or 0.3 *M* sodium acetate: the increase in salt concentration leads to the formation of microcrystals, as revealed by the appearance of Bragg peaks. Insert: scattering curve of 5%(*w*/*v*) PEG 20 000 and 0.3 *M* sodium acetate. The positions of the peaks are in the following ratio: $2^{1/2}$, $6^{1/2}$, $8^{1/2}$, $14^{1/2}$ and $16^{1/2}$. (*b*) Normalized scattering curves of solutions at 20 m*M* sodium acetate, 0.2 *M* sodium acetate and 0.2 *M* sodium acetate containing 5%(*w*/*v*) PEG 20 000, showing the additional attractive effect of PEG.

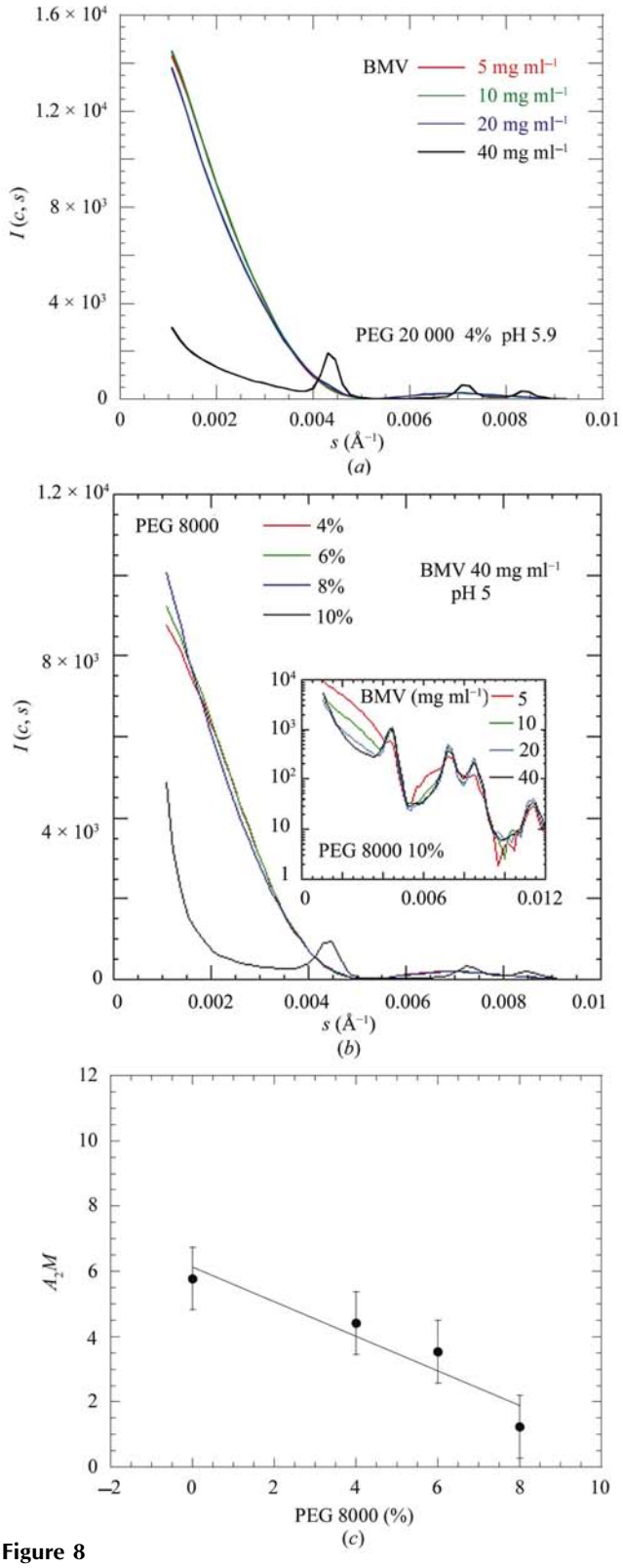

Figure 8
(*a*) Appearance of diffraction peaks in presence of 4%(*w*/*v*) PEG 20 000 with the highest virus concentrations. (*b*) Effects of the increase of PEG 8000 concentration: we see a progressive decrease of the repulsive interactions, leading to the formation of microcrystals. Insert: effects of 10%(*w*/*v*) PEG 8000 with BMV concentrations diluted from 40 to 5 mg ml^{-1}; all the curves present diffraction peaks. (*c*) The interactions become less repulsive with the increase of PEG concentration, as shown by the decrease in A_2 (molecular weight $M = 4.6 \times 10^6$ Da).

the RNA is 95 Å (Jacrot *et al.*, 1977), the gain in volume of the RNA is of about 11%. At low pH values, the interpenetration of the RNA within the protein is important, which leaves a large empty central hole in the centre. At higher pH values, the interpenetration decreases, provoking an increase of the inner volume occupied by the RNA and thus a reduction of the central hole.

At pH 4, a decrease of 35% of the internal radius of the virus was observed when the $NaNO_3$ concentration was increased from 0 to 0.5 *M* $NaNO_3$ (Table 1, Fig. 6*a*), corresponding to a gain of 14% of the RNA volume. It is likely that there is a progressive screening by the anions of the protein basic residues, which no longer interact with the phosphate groups of the RNA. The RNA would then be released from the protein. Moreover, the negatively charged phosphate residues would provoke a swelling of the RNA because of repulsive interaction between them and the consequent radial extension of the RNA.

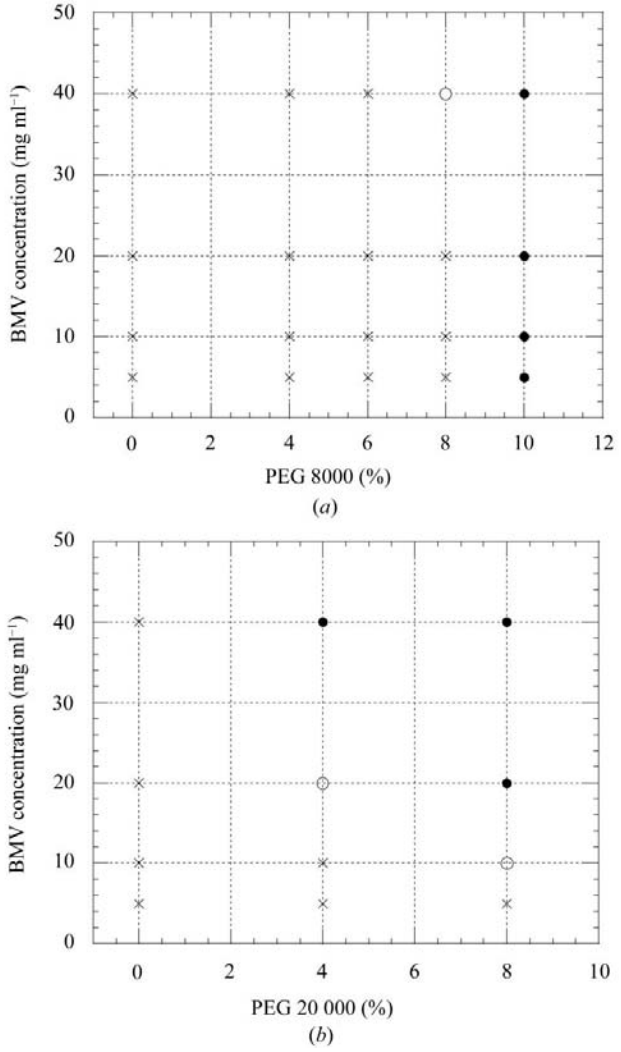

Figure 9
Aspect of SAXS samples immediately after mixing the different components as a function of their PEG 8000 (*a*) or PEG 20 000 (*b*) content (in the presence of 20 m*M* sodium acetate): we observed soluble (crosses), turbid (empty circles) and precipitated (filled circles) samples.

As expected, no structural modification of the virions was observed upon addition of PEG, since this polymer carries no charge.

4.2. Interactions in solution

Varying the pH results in a change of the global charge of the particles, thus influencing the interactions between viruses in solution. In the pH range 4–7.5, the changes in the BMV interactions are a consequence of the successive deprotonation of aspartic acid, glutamic acid and histidine residues, which have respective pK_a values of 3.9, 4.3 and 6.0 when isolated.

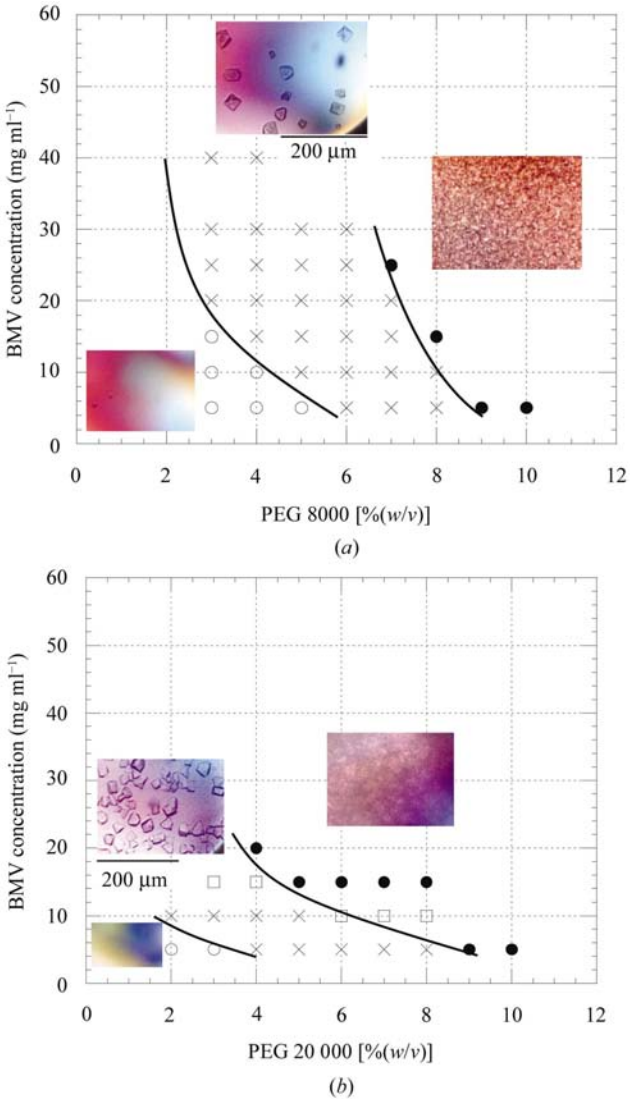

Figure 10
Solubility curves established with microbatch experiments by varying the concentration of BMV from 5 to 40 mg ml^{-1} (in the presence of 20 m*M* sodium acetate), after one week. According to each condition, the wells had either a soluble aspect (empty circles), contained crystals (crosses), contained poor-shaped crystals (empty squares) or had a precipitated aspect (filled circles). (*a*) In the presence of 3–10%(*w*/*v*) PEG 8000 we observed an emergence of numerous small well facetted crystals after 4 d. (*b*) In the presence of 2–10%(*w*/*v*) PEG 20 000, numerous small crystals appeared after a couple of days.

The decrease in the repulsive interactions with the increase of the pH (insert, Fig. 2*b*) is typical for coulombian interactions and indicates that the virus pI is higher than 7.5, *i.e.* basic. The protein has a large number of charged residues (27 basic residues and 17 acid residues), with a pI close to 10; the net charge of the capsid would then be 1800 positive charges. The RNA adds about 3000 charged phosphate residues per virion, leading to a potential net charge of the virion of 1200 negative charges. One would thus have expected higher overall repulsive interactions, even at pH 4.0. This probably reflects the fact that basic residues are interacting with the RNA, since most of them are located inside the capsid in the N-terminal part of the polypeptide chain (seven arginines and one lysine in the 26 N-terminal amino acids); for CCMV, in addition to the equivalent basic residues, 13 other residues were also found to interact with the RNA (Speir *et al.*, 1995). Moreover, nucleic acids are generally stabilized by divalent ions such as Mg^{2+} or Ca^{2+} which we cannot quantify. Finally, at least two glutamic acids involved in the binding of calcium ions and controlling the swelling were found by hydrogen-ion titration to have a shifted pK_a value of 6.5–7 in BMV, CCMV and other $T = 3$ icosahedral viruses (Durham *et al.*, 1977; Jacrot, 1975; Pfeiffer & Durham, 1977), owing to a high local concentration of electronegativity also maintained by distant RNA-phosphate contribution. These residues thus remain protonated. In CCMV, two glutamic acids (Glu81 and Glu148) and one aspartic acid (Asp153) per capsid protein seem to be involved in calcium-binding cages (Speir *et al.*, 1995) close to the quasi-threefold axes of the icosahedral capsid. The sequence identity between the capsid proteins of CCMV and BMV lets us suppose that in BMV three polar residues, Glu81, Glu85 and Asp149, may be involved in calcium ion binding and do not participate in the net charge of the capsid.

In previous studies, the addition of salt was found to induce an additional attraction, specific to the salt type, called the 'Hofmeister effect' (Tardieu *et al.*, 2001). To study whether the differential effect of anions could still be observed with particles of the size of BMV, we tested two monovalent anions, nitrate and acetate, that are at opposite ends of the Hofmeister series. As expected with a complex having a basic pI, nitrate was found to be more effective than acetate. This result indicates that the Hofmeister effect is still important for macromolecules as large as viruses. The screening of the charges seems to be achieved essentially after the addition of 0.2 *M* $NaNO_3$ (Fig. 5*b*), an observation that is consistent with calculations using a DLVO-like interparticle potential. The addition of salt induces structural rearrangements (see below) that seem to increase with ionic strength. Because of this phenomenon, we did not explore the effect of $NaNO_3$ beyond an ionic strength of 0.5 *M*. In this salt range, however, we did not find any conditions where the addition of salt alone was able to induce attractive interactions (see Table 2). In previous studies, the effect was found to induce an attractive regime in solutions of small proteins such as lysozyme, but has been found to be unable to do so with larger proteins such as ATCase and α-crystallins (Bonneté *et al.*, 1999; Budayova *et al.*, 1999; Finet, 1999). The importance of the effect seems to depend upon protein size. In agreement with these results, salt was unable to convert the repulsive interactions of BMV in solution into attractive interactions and to induce crystallization conditions. However, it cannot be ruled out that higher salt concentrations would work, observed for instance with tomato bushy stunt virus, which crystallizes from precipitates in 0.4 to 0.7 *M* ammonium sulfate (Ng *et al.*, 1996).

Fig. 8 shows that the addition of a medium molecular weight PEG (8000) or a high molecular weight PEG (20 000) leads to a progressive decrease of the repulsive interactions, especially at high virus concentration. Our studies show that the addition of PEG, whatever the PEG moelcualr weight, is sufficient to modify BMV interactions in solution to make them almost attractive, even at low ionic strength (20 m*M* sodium acetate). At higher ionic strength (0.1–0.3 *M* for sodium acetate; Fig. 7), this phenomenon is even more pronounced, with a likely synergetic effect as previously observed in the case of ATCase (Budayova *et al.*, 1999).

It was already known that at high concentrations PEG may induce a phase separation with proteins, as well as with macromolecules such as viruses, either liquid–liquid or liquid–solid, where one phase is enriched in PEG and depleted in macromolecules and *vice versa*. When a solid phase is observed, it is usually referred to as a precipitation. This phase separation is sometimes used in the preparation of viruses to obtain a concentrated phase without high-speed centrifugation (Speir *et al.*, 1993). Our studies show that the phase separation is observed as soon as the depletion attraction balances the hard-sphere and electrostatic repulsion.

4.3. Crystallization conditions

If the behaviour of viruses is similar to that of proteins, the solubility curve, that is to say the coexistence curve between the solution and the crystals, should be found for PEG or virus concentrations below the precipitation zone. We thus used conditions close to the SAXS microcrystalline samples for crystallization experiments. To design microbatch experiments, we then used 2–10%(*w*/*v*) PEG 8000 or 20 000 with BMV concentrations varying from 5 to 40 mg ml^{-1}, from which we could establish phase diagrams, representing crystallization and precipitation/microcrystalline zones of BMV concentration as a function of PEG (Fig. 10).

The approach proved to be particularly successful and crystals were obtained from many conditions. The solutions that were macroscopically turbid and which were seen from X-rays to correspond to a mixture of microcrystals and virus in solution were found to produce crystal-like objects. Consequently, the conditions just below the turbid conditions, where the virus were still soluble, provided isolated crystals which were particularly well facetted when using PEG 8000. It is important to notice that although PEG 20 000 is very effective in inducing attraction, it seems to be overly effective and the crystallization zone was narrower. The kinetics of nucleation also seems to be proportional to the PEG-induced attraction.

4.4. Phase diagrams

From a qualitative point of view, it seems that the BMV phase diagram simultaneously presents features observed with proteins and features reminiscent of colloids. With proteins, correlations are now well established between interaction potentials and phase diagrams (Tardieu *et al.*, 2001). Changing interaction conditions towards more attractive ones leads to crystallization. Too strong an attraction, however, may lead to phase separation or precipitation (Lomakin *et al.*, 1999; Malfois *et al.*, 1996). BMV seems to behave in the same way. Upon increasing PEG concentrations, *i.e.* attraction, the phase diagram displays first a crystallization zone and then a precipitation/phase-separation zone. Moreover, as observed with proteins, the kinetics of the two phenomena are rather different. The phase separation occurs in seconds or minutes, whereas nucleation leading to large crystals takes days. As with proteins, one phase is enriched in PEG and depleted in macromolecules and *vice versa* for the other phase. However, at variance with the proteins studied so far, the phase separation induced by PEG or PEG combined with salts is not a fluid–fluid phase separation, metastable with respect to the crystal, but a liquid–solid transition, since the concentrated phase is made of precipitates. This transition has in fact been used for a long time in the preparation of viruses to obtain a concentrated virus phase without using high-speed centrifugation (Speir *et al.*, 1993).

An unexpected and striking result of our experiments is that the PEG-induced precipitates are in fact microcrystals. This transition therefore resembles the liquid to solid/crystal transition observed with colloids when the attraction is short range.

From a more quantitative standpoint, the range of second virial coefficients where BMV crystallization occurs is close to zero yet slightly positive (Figs. 4*b*, 6*c*, 8*c*), whereas the phase separation seems to appear as soon as the depletion attraction balances the hard sphere and electrostatic repulsion. The rapid nucleation of so many microcrystals is also probably an indication that close to the phase separation, the free-energy barrier for crystal nucleation is strongly reduced.

4.5. Nucleation

Classical nucleation theory suggests that for spherical particles the critical nuclei are spherical. However, in recent work, Yau & Vekilov (2000) have reported that with apoferritin, a quasi-spherical protein, the nuclei could be quasi-planar. On the other hand, computer simulations have predicted the occurrence close to critical points of disordered liquid–liquid nuclei with crystallinity appearing at a later stage (ten Wolde & Frenkel, 1997). Whatever the model, the results presented here demonstrate that crystal-like ordering is rapidly established, but of course there is no indication about the shape nor about the size of the critical nuclei themselves. The microcrystals formed in a minute or so, since the diffraction peaks were already visible when the solution was put in the X-ray beam immediately after mixing. They did not seem to grow significantly, as the size of the diffraction peaks did not evolve during the measurement, perhaps because there were not enough viral particles left in the solution. In addition, the microcrystals seem to grow directly from the solution without any other intermediate state. The size of the microcrystals can be estimated to be a few micrometres at most, since the samples look like amorphous precipitates under the light microscope. On the other hand, facetted crystals were seen to appear after a few days. It can therefore be wondered whether there are two different nucleation processes or only one with different kinetic parameters. Finally, in all the conditions where diffraction peaks were observed, the positions of these peaks were conserved, which indicated that the crystal unit-cell remains the same in all the experiments.

We would like to thank Mr P. Dumont and Dr J. M. Camadro who made barley cultivation possible at Jussieu, and the staff of the CMEJ electron-microscopy facility directed by Dr F. Gaill. This work was supported by grants from CNES and from the CNRS-PCV research program.

References

Asakura, S. & Oosawa, F. (1958). *J. Pol. Sci.* **33**, 183.
Atha, D. H. & Ingham, K. C. (1981). *J. Biol. Chem.* **256**, 12108–12117.
Bockstahler, L. E. & Kaesberg, P. (1962). *Biophys. J.* **2**, 1–9.
Bonneté, F., Finet, S. & Tardieu, A. (1999). *J. Cryst. Growth*, **196**, 403–414.
Bonneté, F., Malfois, M., Finet, S., Tardieu, A., Lafont, S. & Veesler, S. (1997). *Acta Cryst.* D**53**, 438–447.
Bonneté, F., Vivares, D., Robert, C. & Colloc'h, N. (2001). In the press.
Boyer, M., Roy, M.-O., Jullien, M., Bonneté, F. & Tardieu, A. (1999). *J. Cryst. Growth*, **196**, 185–192.
Brisco, M., Hull, R. & Wilson, T. M. A. (1986). *Virology*, **148**, 210–217.
Budayova, M., Bonneté, F., Tardieu, A. & Vachette, P. (1999). *J. Cryst. Growth*, **196**, 210–219.
Chauvin, C., Pfeiffer, P., Witz, J. & Jacrot, B. (1978). *Virology*, **88**, 138–148.
Chidlow, J. & Tremaine, J. H. (1971). *Virology*, **43**, 267–278.
Cuillel, M., Jacrot, B. & Zulauf, M. (1981). *Virology*, **110**, 63–72.
Derjaguin, B. (1940). *Trans. Faraday Soc.* **36**, 203.
Dubuisson, J. M., Decamps, T. & Vachette, P. (1997). *J. Appl. Cryst.* **30**, 49–54.
Ducruix, A., Guilloteau, J. P., Riès-Kautt, M. & Tardieu, A. (1996). *J. Cryst. Growth*, **168**, 28–39.
Durham, A. C., Hendry, D. A. & Von Wechmar, M. B. (1977). *Virology*, **77**, 524–33.
Feigin, L. A. & Svergun, D. I. (1987). *Structure Analysis by Small-Angle X-ray and Neutron Scattering.* New York: Plenum Press.
Finet, S. (1999). PhD thesis. Université Pierre et Marie Curie, Paris, France.
Finet, S. & Tardieu, A. (2001). In the press.
George, A. & Wilson, W. W. (1994). *Acta Cryst.* D**50**, 361–365.
Guo, B., Kao, S., McDonald, H., Asanov, A., Combs, L. L. & Wilson, W. W. (1999). *J. Cryst. Growth*, **196**, 424–433.
Haas, C., Drenth, J. & Wilson, W. W. (1999). *J. Phys. Chem.* **103**, 2808–2811.
Hofmeister, F. (1888). *Arch. Exp. Pathol. Pharmakol.* **24**, 247–260.
Incardona, N. L. & Kaesberg, P. (1964). *Biophys. J.* **4**, 11–21.
Israelachvili, J. (1994). *Intermolecular and Surface Forces*. New York: Academic Press.
Jacrot, B. (1975). *J. Mol. Biol.* **95**, 433–446.

Jacrot, B., Chauvin, C. & Witz, J. (1977). *Nature (London)*, **266**, 417–421.
Krol, M. A., Olson, N. H., Tate, J., Johnson, J. E., Baker, T. S. & Ahlquist, P. (1999). *Proc. Natl Acad. Sci. USA*, **96**, 13650–13655.
Kulkarni, A. M., Chatterjee, A. P., Schweizer, K. S. & Zukoski, C. F. (2000). *J. Chem. Phys.* **113**, 9863–9873.
Lafont, S., Veesler, S., Astier, J.-P. & Boistelle, R. (1997). *J. Cryst. Growth*, 173, 132–140.
Lomakin, A., Asherie, N. & Benedek, G. B. (1999). *Proc. Natl Acad. Sci. USA*, **96**, 9465–9468.
Luzzati, V. & Tardieu, A. (1980). *Annu. Rev. Biophys. Bioeng.* **9**, 1–29.
Malfois, M., Bonneté, F., Belloni, L. & Tardieu, A. (1996). *J. Chem. Phys.* **105**, 3290–3300.
Malkin, A. J. & McPherson, A. (1993). *J. Cryst. Growth*, **128**, 1232–1235.
Muschol, M. & Rosenberger, F. (1995). *J. Chem. Phys.* **103**, 10424–10432.
Ng, J. D., Lorber, B., Witz, J., Théobald-Dietrich, A., Kern, D. & Giegé, R. (1996). *J. Cryst. Growth*, **168**, 50–62.
Perez, J., Defrenne, S., Witz, J. & Vachette, P. (2000). *Cell Mol. Biol.* **46**, 937–948.
Petsev, D. N. & Vekilov, P. G. (2000). *Phys. Rev. Lett.* **84**, 1339–1342.
Pfeiffer, P. & Durham, A. C. (1977). *Virology*, **81**, 419–432.
Pfeiffer, P. & Hirth, L. (1974). *Virology*, **61**, 160–167.
Poon, W., Pusey, P. & Lekkerkerker, H. (1996). *Phys. World*, 27–32.
Speir, J. A., Munshi, S., Baker, T. S. & Johnson, J. E. (1993). *Virology*, **193**, 234–241.
Speir, J. A., Munshi, S., Wang, G., Baker, T. S. & Johnson, J. E. (1995). *Structure*, **3**, 63–78.
Svergun, D. & Semenyuk, A. (1993). *GNOM: Small-Angle Scattering Data Processing by Means of Regularization Technique.* Moscow, Russia: Institute of Crystallography, Academy of Sciences of Russia.
Tardieu, A. (1994). In *Neutron and Synchrotron Radiation for Condensed Matter Studies*, edited by J. L. H. J. Baruchel, M. S. Lehman, J. R. Regnard & C. Schlenker, p. 145. Berlin: Springer.
Tardieu, A., Finet, S. & Bonneté, F. (2001). In the press.
Tardieu, A., Le Verge, A., Malfois, M., Bonneté, F., Finet, S., Riès-Kautt, M. & Belloni, L. (1999). *J. Cryst. Growth*, **196**, 193–203.
Veesler, S., Lafont, S., Marcq, S., Astier, J.-P. & Boistelle, R. (1996). *J. Cryst. Growth*, **168**, 124–129.
Velev, O. D., Kaler, E. W. & Lenhoff, A. M. (1998). *Biophys. J.* **75**, 2682–97.
Verwey, E. J. W., Overbeek, J. T. G. & van Nes, K. (1948). *Theory of the Stability of Lyophobic Colloids*, p. 205. Amsterdam: Elsevier.
Wolde, P. R. ten & Frenkel, D. (1997). *Science*, **277**, 1975–1978.
Yau, S. T. & Vekilov, P. G. (2000). *Nature (London)*, **406**, 494–497.
Ye, X., Narayanan, T., Tong, P., Huang, J. S., Lin, M. Y., Carvalho, B. L. & Fetters, L. J. (1996). *Phys. Rev. E*, **54**, 6500–6510.
Zulauf, M., Cuillel, M. & Jacrot, B. (1983). *Scattering Techniques Applied to Supramolecular and Nonequilibrium Systems: Neutron and Light Scattering Studies of Brome Mosaic Virus and its Protein*, pp. 865–871. New York/London: Plenum Press.